Nonconservative dynamics of optically trapped high-aspect-ratio nanowires

Wen Jun Toe,[1] Ignacio Ortega-Piwonka,[2] Christopher N. Angstmann,[2] Qiang Gao,[3] Hark Hoe Tan,[3] Chennupati Jagadish,[3] Bruce I. Henry,[2] and Peter J. Reece[1,*]

[1]*School of Physics, The University of New South Wales, Sydney NSW 2052, Australia*
[2]*School of Mathematics and Statistics, The University of New South Wales, Sydney NSW 2052, Australia*
[3]*Research School of Physics and Engineering, The Australian National University, Canberra ACT 2601, Australia*

We investigate the dynamics of high-aspect-ratio nanowires trapped axially in a single gradient force optical tweezers. A power spectrum analysis of the dynamics reveals a broad spectral resonance of the order of kHz with peak properties that are strongly dependent on the input trapping power. A dynamical model incorporating linear restoring optical forces, a nonconservative asymmetric coupling between translational and rotational degrees of freedom, viscous drag, and white noise provides an excellent fit to experimental observations. A persistent low-frequency cyclical motion around the equilibrium trapping position, with a frequency distinct from the spectral resonance, is observed from the time series data.

I. INTRODUCTION

Optical trapping studies of low-symmetry objects, such as rods, ellipsoids, and oblate spheroids, provide new dimensions to the study of optical trapping dynamics. In addition to more complex hydrodynamic interactions, nonspherical objects are subject to preferential trapping orientations and associated restoring torques when displaced away from equilibrium. When the trapping point is positioned arbitrarily with respect to the geometric center, perturbative forces can lead to complex cross-coupling between translational and rotational motion [1]. Shape mediated effects have been discussed in the context of tailored optical force profiles, including the generation of optical lift [2] and negative radiation pressure [3], and have consequently been implemented in a practical setting for passive force clamping in photonic force microscopy [4].

One interesting peculiarity that has seen growing attention is the tendency of low-symmetry particles to undergo persistent oscillatory motion in thermal equilibrium. This type of motion was first articulated for optically trapped rods by Simpson and Hanna, where it was related to the influence of nonconservative optical scattering forces, inducing coupling between rotation and translation [5]. The concept has its genesis in an earlier study by Roichman *et al.* who explored the influence of the nonconservative scattering force in producing circulating currents in the stochastic trajectories of spherical particles in an optical tweezers [6]. These concepts have been extended by Saberi and Gittes who consider general nonconservative forcing effects in optical tweezers [7].

Our interests lie in experimental investigations of weakly tapered, high refractive index, indium phosphide (InP) nanowires of uniform composition, held in a linearly polarized, gradient force optical tweezers [8]. Nanowires are a particular subclass of nonspherical objects with nanoscale radial dimensions and lengths that extend to several micrometers, giving aspect ratios in excess of 100:1. For trapping experiments, the extended axial dimension can exceed the depth of focus of the trapping beams by several times the Rayleigh range, thereby

creating a trapping force that is localized to a particular point on the axis. Earlier studies have shown that the equilibrium trapping position of these nanowires has been determined to be near one end, with the major segment of the length sitting below the trap far from the geometric center [9], which is qualitatively consistent with modeling of tapered rods [10]. The optically trapped nanowires are aligned closely to the optical axis of the tweezers and experience small perturbations from the equilibrium point due to stochastic motion. Note that these trapping conditions exclude the possibility of major orientation changes that are observed in other studies [11,12].

Here we present experimental evidence for the presence of resonant fluctuations in the stochastic motion of optically trapped nanowires. A power spectral density analysis of the nanowire motion reveals a broad resonance peak of the of the order of kHz with characteristics dependent on the input trapping power and the trapping height above the coverslip. A dynamical model is constructed with the following features: linear restoring optical forces acting at an equilibrium trapping point on the rod; an additional nonconservative force providing asymmetric coupling between translational and rotational degrees of freedom; a viscous drag applied at a point on the rod; and white noise accounting for the random fluctuations of the fluid. This model provides an excellent fit to experimental observations of the power spectra. Further, a winding number analysis of the positional time series reveals clear cyclical motion around the trapping point.

II. METHOD

Our experimental apparatus consists of a single beam gradient force optical trap generated at the focus of a high numerical aperture oil immersion microscope objective lens (Nikon E Plan Achromat 100x 1.25NA) using a Nd:YAG laser emitting at 1064 nm (Laser Quantum IR Ventus). Dynamic steering of the laser focus is provided by a two-axis acousto-optic deflector (AOD) (Gooch and Housego 45035 AOBD) and spatial light modulator (SLM) (Hamamatsu LCOS-SLM x10468-03) positioned within the optical train at planes conjugate with the back aperture of the objective. SLM-based aberration correction and overfilling of the back aperture are
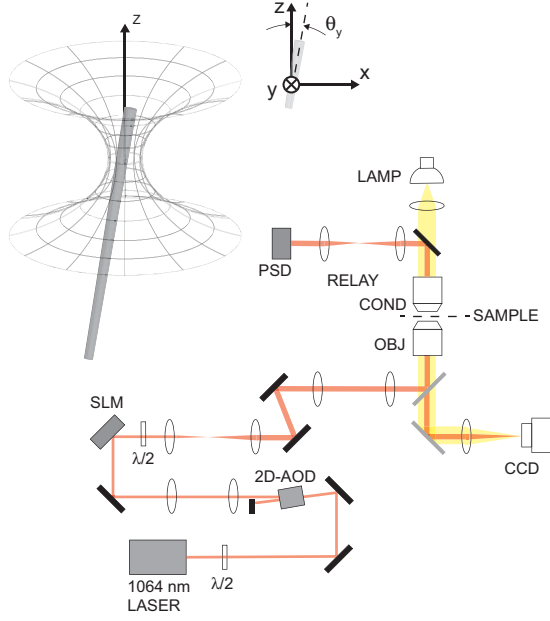
*p.reece@unsw.edu.au

FIG. 1. Schematic of our experimental setup and geometry within the optical trap with relevant coordinates and angles. In the experimental arrangement a diode pumped solid state laser is used with adaptive optics to create a diffraction limited spot within the focal plane of the objective (OBJ). The nanowires are trapped near the end of the wire and aligned along the laser axis. Light scattering from the nanowire is collected by the condenser (COND) and used to perform back focal plane interferometry with a position sensitive detector (PSD).

used to produce a diffraction limited spot optimized for optical trapping. The power of the trapping laser at the imaging plane is controlled by the AOD and set between 10 and 90 mW. A schematic diagram of the trapping arrangement is shown in Fig. 1.

The indium phosphide (InP) nanowires used in the study are epitaxially grown on InP (111)B substrates by metal-organic chemical vapor deposition (MOCVD) using gold nanoparticle catalysts. The nanowires are between 5 and 10 μm have a tapered aspect of approximately $0.3°$ as characterized by electron microscopy. Further information on the growth process can be found elsewhere [13].

For tweezers measurements, the nanowires are dispersed into an aqueous solution by sonication and transferred to a hermetically sealed chamber at a dilution where single nanowires can be isolated. Visualizing the nanowires in the trap is achieved using a charge-coupled device (CCD) camera (AVT Stingray) together with diascopic illumination supplied by the condenser. Back focal plane interferometry is performed by collecting the forward scattered light from the trapped nanowires with a high numerical aperture condenser lens (Olympus S Plan Fluor 40x 0.6NA) and projected onto a position sensitive diode (PSD) (Pacific Sensor, DL16-7PCBA) located at a conjugate plane to the condenser back aperture. The PSD is connected to a field-programmable gate array (FPGA) multifunction acquisition card (National Instruments PCIe-7852R) and time series measurements of the nanowire position fluctuation with respect to the trapping center are

recorded at a sampling rate of 10 kHz for a period of 10 s. The linearity of the PSD detector response with respect to the nanowire position in this orientation has been previously verified [8].

III. THEORY

We treat the nanowire as a rigid body in the shape of a conical frustum. The stochastic motion of the nanowire within an optical trap can be described by a set of Langevin equations in terms of translational (x,y,z) and angular coordinates $(\theta_x,\theta_y,\theta_z)$. These co-ordinates are shown schematically in Fig. 2.

We assume that the optical tweezers give rise to linear restoring forces that operate through the point (x,y,z). We refer to this point as the trapping point on the nanowire. We also assume that the optical tweezers give rise to linear restoring torques about the trapping point in the angles (θ_x,θ_y). The trapping point is typically near the large radius end of the tapered nanowire, above the position of the center of mass [9]. We also consider the possibility of a nonconservative linear force in the x and y directions proportional to θ_y, and θ_x, respectively. The total linearized optical force at the trapping point is given by

$$\mathbf{F}_{\mathrm{O}} = \begin{pmatrix} F_x \\ F_y \\ F_z \end{pmatrix} = - \begin{pmatrix} k_x x + c_y \theta_y \\ k_y y + c_x \theta_x \\ k_z z \end{pmatrix}, \qquad (1)$$

where k_x, k_y, k_z are positive but there is no restriction on the sign of c_x or c_y. The restoring torque about the trapping point is taken to be

$$\mathcal{T}_{\mathrm{O}} = \begin{pmatrix} \mathcal{T}_{\theta_x} \\ \mathcal{T}_{\theta_y} \\ \mathcal{T}_{\theta_z} \end{pmatrix} = - \begin{pmatrix} k_{\theta_x}\theta_x \\ k_{\theta_y}\theta_y \\ 0 \end{pmatrix}. \qquad (2)$$

The motion of the nanowire is opposed by a viscous drag that depends on nanowire's shape and surface area. We assume that there is a center of drag, also called a center of hydrodynamics stress [14], and the viscous drag operates through this point. We further assume that the center of drag is distinct from the trapping point. This is a reasonable
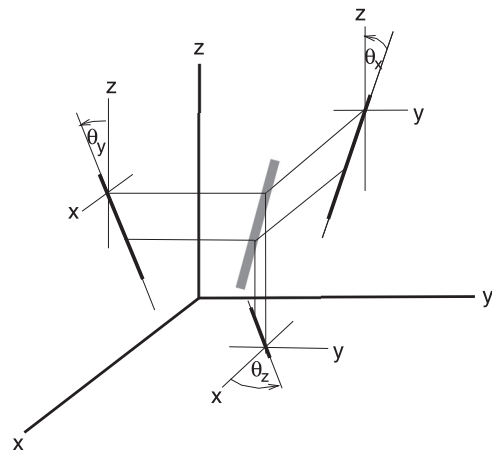

FIG. 2. Schematic illustration of the coordinate system used in the model for the dynamics of the nanowire.

assumption given that the trapping point is typically above the center of mass, and the surface area is balanced at a point below the center of mass for a conical frustum. With the above assumptions, neglecting inertial effects in the overdamped limit, the optical forces acting through the trapping position would induce a torque about the center of drag. We label the center of drag by coordinates (u,v,w) and in the small angle approximation we have

$$
\begin{aligned}
x &= u + \ell\theta_y, \\
y &= v - \ell\theta_x, \\
z &= w + \ell,
\end{aligned}
\tag{3}
$$

where ℓ is the distance between the center of drag and the trapping position. The induced torque is given by

$$
\mathcal{T}_\mathrm{D} = \begin{pmatrix} \mathcal{T}_u \\ \mathcal{T}_v \\ \mathcal{T}_w \end{pmatrix} = \mathbf{r} \times \mathbf{F}_\mathrm{O},
$$

where $\mathbf{r} = (x - u, y - v, z - w)^T$. Explicitly, retaining terms that are linear in the coordinates $x, y, z, \theta_x, \theta_y$, and then using the transformations in Eq. (3) we have

$$
\mathcal{T}_\mathrm{D} = \begin{pmatrix} \ell k_y y + \ell c_x \theta_x \\ -\ell k_x x - \ell c_y \theta_y \\ 0 \end{pmatrix} = \begin{pmatrix} \ell k_y v - \ell^2 k_y \theta_x + \ell c_x \theta_x \\ -\ell k_x u - \ell^2 k_x \theta_y - \ell c_y \theta_y \\ 0 \end{pmatrix}.
\tag{4}
$$

Using the transformations in Eq. (3) we can express the optical force in the center of drag coordinates as

$$
\mathbf{F}_\mathrm{O} = \begin{pmatrix} F_u \\ F_v \\ F_w \end{pmatrix} = - \begin{pmatrix} k_x u + k_x \ell\theta_y + c_y \theta_y \\ k_y v - k_y \ell\theta_x + c_x \theta_x \\ k_z w + k_z \ell \end{pmatrix}.
\tag{5}
$$

We can combine the above optical forces and torques in a single vector as follows:

$$
\mathbf{G}_\mathrm{O} = \begin{pmatrix} G_u \\ G_{\theta_y} \\ G_v \\ G_{\theta_x} \\ G_w \\ G_{\theta_z} \end{pmatrix} = \begin{pmatrix} F_u \\ \tau_v + \tau_{\theta_y} \\ F_v \\ \tau_u + \tau_{\theta_x} \\ F_w \\ \tau_w + \tau_{\theta_z} \end{pmatrix}.
\tag{6}
$$

Given that G_{θ_z} is zero we ignore motion in the θ_z coordinate in the following.

Finally we include the drag proportional to the velocity of the center of drag and we include independent white noise terms in each of the coordinates with zero mean, and variance given by the Einstein relation for kinetic theory. This results in the dynamical equation

$$
-\Gamma\dot{\delta\vec{q}} + \vec{\zeta}(t) - \mathbf{K}\delta\vec{q} = \vec{0},
\tag{7}
$$

where $\delta\vec{q} = (\delta u, \delta\theta_y, \delta v, \delta\theta_x, \delta w)^T$ is a generalized coordinate vector, representing small displacements around the equilibrium values $u^* = 0$, $\theta_y^* = 0$, $v^* = 0$, $\theta_x^* = 0$, and $w^* = -\ell$. The drag matrix is assumed to be diagonal in the center of

drag coordinates, so that

$$
\Gamma = \begin{pmatrix} \gamma_u & 0 & 0 & 0 & 0 \\ 0 & \gamma_{\theta_y} & 0 & 0 & 0 \\ 0 & 0 & \gamma_v & 0 & 0 \\ 0 & 0 & 0 & \gamma_{\theta_x} & 0 \\ 0 & 0 & 0 & 0 & \gamma_w \end{pmatrix}.
\tag{8}
$$

The white noise vector $\vec{\zeta}(t) = (\zeta_u, \zeta_{\theta_y}, \zeta_v, \zeta_{\theta_x}, \zeta_w)^T$ has the expected value $\langle \zeta_i(t) \rangle = 0$ and correlations $\langle \zeta_i(t)\zeta_j(t + \tau) \rangle = 2 k_b T \gamma_i \delta_{ij} \delta(\tau)$. The matrix $\mathbf{K}$ is the optical stiffness matrix defined by $-\mathbf{K}\delta\vec{q} = \mathbf{G}_\mathrm{O}$ with $\mathbf{G}_O$ evaluated at $u = u^* + \delta u$, $\theta_y = \theta_y^* + \delta\theta_y$, $v = v^* + \delta v$, $\theta_x = \theta_x^* + \delta\theta_x$, and $w = w^* + \delta w$. Substituting Eqs. (2), (4), and (5) into Eq. (6) evaluated at $\vec{q} = \vec{q}^* + \delta\vec{q}$, we have

$$
\mathbf{K} = \begin{pmatrix} k_x & \ell k_x + c_y & 0 & 0 & 0 \\ \ell k_x & \ell^2 k_x + \ell c_y + k_{\theta_y} & 0 & 0 & 0 \\ 0 & 0 & k_y & -\ell k_y + c_x & 0 \\ 0 & 0 & -\ell k_y & \ell^2 k_y - \ell c_x + k_{\theta_x} & 0 \\ 0 & 0 & 0 & 0 & k_z \end{pmatrix}.
\tag{9}
$$

The experimental observations on the motion of the nanowire are the position co-ordinates, $\hat{x}, \hat{y}, \hat{z}$ near the uppermost tip, a distance $\hat{\ell}$ above the center of drag. We let $\hat{\delta\vec{q}} = (\hat{\delta}x, \delta\theta_y, \hat{\delta}y, \delta\theta_x, \hat{\delta}z)^T$ denote the generalized coordinates of the observation point. The dynamical equation in the observed coordinates can be found using the linear transformation $\hat{\delta\vec{q}} = \mathbf{J}\delta\vec{q}$ with

$$
\mathbf{J} = \begin{pmatrix} 1 & \hat{\ell} & 0 & 0 & 0 \\ 0 & 1 & 0 & 0 & 0 \\ 0 & 0 & 1 & -\hat{\ell} & 0 \\ 0 & 0 & 0 & 1 & 0 \\ 0 & 0 & 0 & 0 & 1 \end{pmatrix}.
\tag{10}
$$

Substituting the linear transformation into Eq. (7) we obtain the equations of motion

$$
\frac{d\hat{\delta\vec{q}}}{dt} = -\mathbf{M}\hat{\delta\vec{q}} + \vec{\xi}(t),
\tag{11}
$$

where

$$
\mathbf{M} = \mathbf{J}\Gamma^{-1}\mathbf{K}\mathbf{J}^{-1}
\tag{12}
$$

and

$$
\vec{\xi}(t) = \mathbf{J}\Gamma^{-1}\vec{\zeta}(t).
\tag{13}
$$

It is easy to verify that $\mathbf{M}$ has the block structure

$$
\mathbf{M} = \begin{pmatrix} M_{x,x} & M_{x,\theta_y} & 0 & 0 & 0 \\ M_{\theta_y,x} & M_{\theta_y,\theta_y} & 0 & 0 & 0 \\ 0 & 0 & M_{y,y} & M_{y,\theta_x} & 0 \\ 0 & 0 & M_{\theta_x,y} & M_{\theta_x,\theta_x} & 0 \\ 0 & 0 & 0 & 0 & M_{z,z} \end{pmatrix},
\tag{14}
$$

where

$$M_{x,x} = \frac{k_x}{\gamma_u} + \hat{\ell} M_{\theta_y,x},$$

$$M_{x,\theta_y} = \frac{-\hat{\ell} k_x + k_x \ell + c_y}{\gamma_u} + \hat{\ell} M_{\theta_y,\theta_y},$$

$$M_{\theta_y,x} = \frac{\ell k_x}{\gamma_{\theta_y}},$$

$$M_{\theta_y,\theta_y} = \frac{-\hat{\ell} k_x \ell + k_x \ell^2 + c_y \ell + k_{\theta_y}}{\gamma_{\theta_y}},$$

$$M_{y,y} = \frac{k_y}{\gamma_v} - \hat{\ell} M_{\theta_x,y},$$

$$M_{y,\theta_x} = \frac{\hat{\ell} k_y - k_y \ell + c_x}{\gamma_v} - \hat{\ell} M_{\theta_x,\theta_x},$$

$$M_{\theta_x,y} = -\frac{\ell k_y}{\gamma_{\theta_x}},$$

$$M_{\theta_x,\theta_x} = \frac{-\hat{\ell} k_y \ell + k_y \ell^2 - c_x \ell + k_{\theta_x}}{\gamma_{\theta_x}},$$

$$M_{z,z} = \frac{k_z}{\gamma_w}.$$

The above approximations thus lead to a description of the dynamics in three sets of coupled equations of motion that describe the dynamics over the XZ plane (x,θ_y), the YZ plane (y,θ_x), and the z axis. These subsystems retain the nonconservative effects and can be treated independently. For example, the two equations that describe the dynamics in the YZ plane can be written explicitly as

$$\frac{d\hat{\delta} y}{dt} = -M_{y,y}\hat{\delta} y - M_{y,\theta_x}\delta\theta_x + \frac{1}{\gamma_v}\zeta_v(t) - \frac{\hat{\ell}}{\gamma_{\theta_x}}\zeta_{\theta_x}(t), \quad (15)$$

$$\frac{d\delta\theta_x}{dt} = -M_{\theta_x,y}\hat{\delta} y - M_{\theta_x,\theta_x}\delta\theta_x + \frac{1}{\gamma_{\theta_x}}\zeta_{\theta_x}(t). \quad (16)$$

This system can be written in vector form as

$$\frac{d\vec{\psi}}{dt} = \mathbf{A}\vec{\psi} + \mathbf{L}\vec{\zeta}, \quad (17)$$

where

$$\vec{\psi} = \begin{pmatrix} \delta y \\ \delta\theta_x \end{pmatrix}, \quad (18)$$

$$\mathbf{A} = \begin{pmatrix} -M_{y,y} & -M_{y,\theta_x} \\ -M_{\theta_x,y} & -M_{\theta_x,\theta_x} \end{pmatrix}, \quad (19)$$

and

$$\mathbf{L} = \begin{pmatrix} \frac{1}{\gamma_v} & -\frac{\hat{\ell}}{\gamma_{\theta_x}} \\ 0 & \frac{1}{\gamma_{\theta_x}} \end{pmatrix}. \quad (20)$$

The power spectrum for this system can be written as [15]

$$\mathbf{S}(\omega) = (\mathbf{A} - i\omega\mathbf{I})^{-1}\mathbf{L}\mathbf{Q}\mathbf{L}^T(\mathbf{A} + i\omega\mathbf{I})^{-T}, \quad (21)$$

where $\mathbf{I}$ is the 2×2 identity matrix and

$$\mathbf{Q} = \begin{pmatrix} \eta_v & 0 \\ 0 & \eta_{\theta_x} \end{pmatrix}, \quad (22)$$

with $\eta_i = 2k_B T\gamma_i$.

This leads to a power spectral density for each coupled coordinate that has the form

$$S_i(\omega) = \frac{\alpha_i\omega^2 + \beta_i}{(\omega^2 - \epsilon)^2 + (\mu\omega)^2}, \quad (23)$$

where

$$\mu = \frac{-k_y\ell^2}{\gamma_{\theta_x}} + \frac{c_x\ell}{\gamma_{\theta_x}} - \frac{k_y}{\gamma_v} - \frac{k_{\theta_x}}{\gamma_{\theta_x}} \quad (24)$$

is the trace of the matrix $\mathbf{A}$,

$$\epsilon = \frac{k_y k_{\theta_x}}{\gamma_{\theta_x}\gamma_v} \quad (25)$$

is the determinant of the matrix $\mathbf{A}$, and α_i and β_i are positive parameters arising from the white noise at the center of drag. For example

$$\alpha_y = \frac{\hat{\ell}^2\eta_{\theta_x}}{\gamma_{\theta_x}^2} + \frac{\eta_v}{\gamma_v^2}, \quad (26)$$

and

$$\beta_y = \frac{[k_{\theta_x} - (c_x + \hat{\ell}k_y)\ell + k_y\ell^2]^2\eta_v + [c_x + k_y(\hat{\ell} - \ell)]^2\eta_{\theta_x}}{\gamma_v^2\gamma_{\theta_x}^2}. \quad (27)$$

We note that the equilibrium solution of Eq. (17) is unstable if $\mu > 0$ and this places a constraint on the size of the nonconservative coupling in this model.

To allow for detector noise in the experimental measurements of the power spectrum we carry out fits below based on the functional form

$$S_i(\omega) = \frac{\alpha_i\omega^2 + \beta_i}{(\omega^2 - \epsilon)^2 + (\mu\omega)^2} + \sigma_i, \quad (28)$$

This functional form has a maximum at a nonzero frequency

$$\omega^* = \sqrt{\sqrt{\left(\epsilon + \frac{\beta_i}{\alpha_i}\right)^2 - \frac{\beta_i}{\alpha_i}\mu^2} - \frac{\beta_i}{\alpha_i}} \quad (29)$$

provided that

$$\epsilon > \frac{2\beta_i}{\alpha_i}\left(\sqrt{1 + \frac{\alpha_i}{\beta_i}\mu^2} - 1\right). \quad (30)$$

If $\epsilon \gg |\mu|$ then

$$\omega^* \sim \sqrt{\epsilon} - \frac{1}{4}\left(\frac{\beta_i}{\alpha_i}\right)\mu^2\left(\frac{1}{\epsilon}\right)^{3/2}. \quad (31)$$

IV. RESULTS

In Fig. 3 we present experimental measurements of the power spectrum from a typical nanowire trapped at different trapping heights above the chamber. The figure also shows fits based on Eq. (28) with parameters as shown in Table I.

The physical dimensions of the nanowire are approximately 50 nm by 5 μm in length, Fig. 3(c) inset. The power spectrum
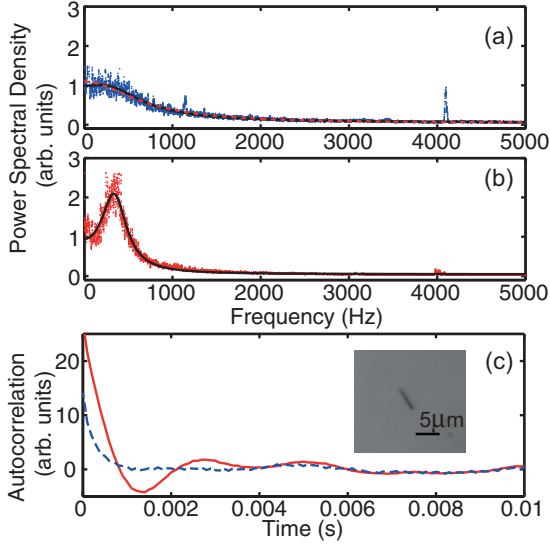
FIG. 3. (a) Experimental power spectrum of a nanowire trapped approximately 10 μm from the cover slip (blue dots). The dashed (red) line is a Lorentzian fit which is characteristic of Brownian dynamics in an optical trap; and the solid (black) is the presented model. (b) Experimental power spectrum of the same nanowire trapped approximately 50 μm from the cover slip (red dots). The solid (black) line is the fitted spectrum from the presented model. (c) Autocorrelation function of the nanowire motion approximately 10 μm from the cover slip (dashed) and approximately 50 μm from the cover slip (solid). The inset is a bright field image of the untrapped nanowire.

in Fig. 3(a) was recorded when the nanowire was trapped at a height of approximately 10 μm and is plotted together with two fits; a Lorentzian (dashed), which is consistent with uncoupled dynamics [16], and our model power spectrum, Eq. (28). We do not observe a second Lorentzian component in the power spectrum corresponding to the rotation dynamics, however from previous work analyzing autocorrelation data it is noted that the characteristic frequency for rotation is somewhat smaller compared with the translation motion [17]. When the trapping height above the cover slip is increased to approximately 50 μm a broad resonant peak is apparent in the power spectrum (red), shown in Fig. 3(b). The fit of the power spectrum using Eq. (28) shows excellent agreement with the experimental data. The resonance is also observed in the autocorrelation function of the nanowire trajectory, where a fluctuation between a positive and negative correlation can be seen, as shown in Fig. 3(c). A fit of the data taken at the lower trapping height Fig. 3(a) also reveals a strongly suppressed peak at a similar frequency. The full height of the chamber is estimated to be in excess of 100 μm and so we exclude the

possibility of direct interaction with the chamber walls. We note that changing the height of the trap will induce spherical aberrations and accentuate other aberrations already present within the trap. Increased aberrations will change the relative contributions from gradient and scattering forces for a given fixed input power, and this may be implicated in the height dependence of the resonance. Given that the theoretical model provides a good fit to the power spectrum at both trapping heights it is reasonable to assume that the height dependence may be incorporated into the model through different values of system parameters. The lack of an explicit dependence in the model prohibits predictions of the resonant peak in the power spectrum with the variation in trapping height so that this remains an empirical observation.

From the experimental measurements and theoretical fits we can make the following observations: (i) The model reduces to a Lorentzian when $c_x = 0, c_y = 0, \ell = 0$, i.e., there is no nonconservative optical force and there is no induced torque from the drag, independent of the experimental observation point $\hat{\ell}$. (ii) A nonzero peak can occur when there is a nonconservative optical force and induced drag provided that Eq. (30) is satisfied. (iii) The increase in the position of the resonance peak ω^* is correlated with a decrease in μ^2, Eq. (29). This may correspond to a decrease in the restoring forces and torques, or a decrease in the distance between the center of drag and the trapping position, Eq. (24). Both of these possibilities are consistent with increased optical aberrations with depth. (iv) The height of the peak increases with increasing α.

To further investigate the dynamics of the resonance, the power spectrum of a trapped nanowire of length 4.6 μm was
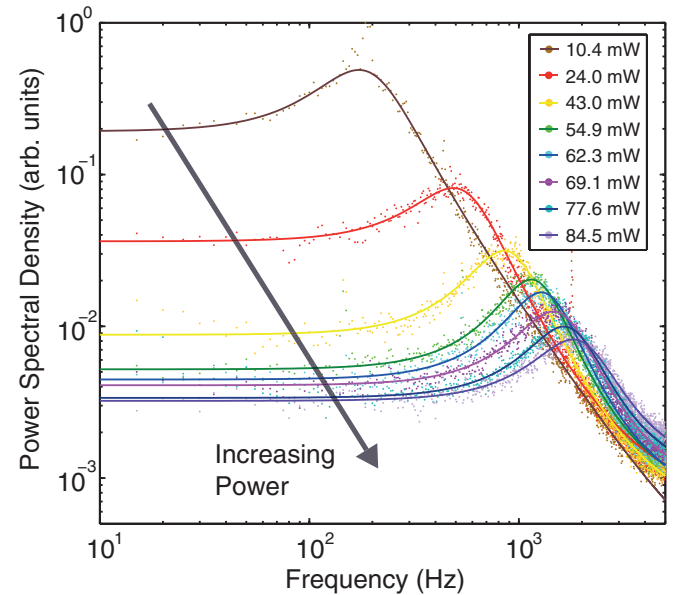

FIG. 4. Power spectral density of a single nanowires held at a fixed trapping power measured for different trapping powers. The peak frequency shifts given by the $\sqrt{\epsilon}$ increases linearly with trapping power, while the Brownian fluctuations are strongly suppressed. The solid lines represent the fitted model which includes nonconservative cross-coupling between translation and rotation. The arrow indicates how the power spectral density changes with increasing trapping power.
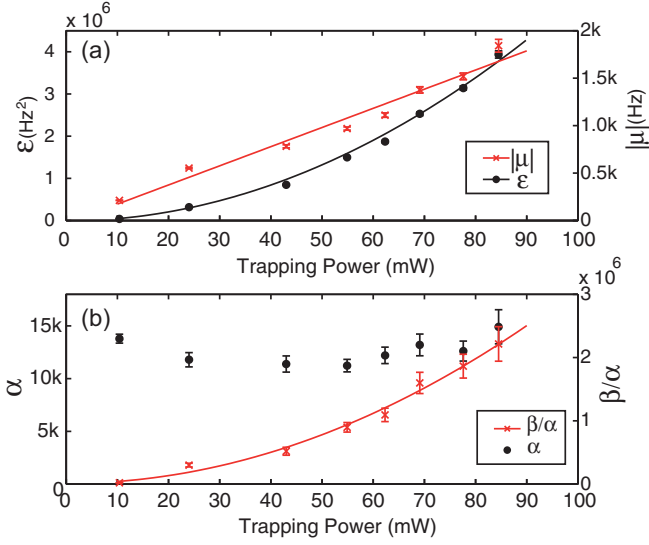
TABLE I. Fitting parameters for power spectrum at different trapping heights.

Height (μm)	ϵ (Hz^2)	$|\mu|$(Hz)	β/α	α	σ
~10	1.76×10^5	843	7.06×10^4	4.08×10^5	0.048
~50	1.53×10^5	350	2.43×10^5	8.94×10^4	0.044

FIG. 5. Fitting parameters of the power spectral density data presented in Fig 4. (a) ϵ increase quadratically and μ linearly with trapping power, which corresponds to linear increase in both the peak frequency and width. (b) The noise strength α shows no clear dependence on trapping power indicating a constant temperature, while β/α increases quadratically with trapping power. All dependencies are consistent with a trap stiffness that is linearly proportional to the trapping intensity in the presence of asymmetric coupling.

recorded as a function of input trapping laser powers ranging from 10 to 90 mW. The power dependent results are presented in Fig. 4 along with the associated fits using Eq. (28); again we note exceptional agreements between experimental results and the model. Qualitatively we see that the peak position of the resonance is blueshifted from 200 to 1800 Hz with increasing trapping power together with a reduction of the amplitude of the fluctuations. The parameters associated with the fits are given in Fig. 5. We observe that ϵ increases quadratically with trapping power, while $|\mu|$ increases linearly. This is consistent with the model equations, Eqs. (25) and (24), under the assumption that the trap stiffness parameters k_i scale linearly with power. The parameter α is observed to be roughly constant across all trapping powers, which indicates that there is no obvious heating across the different trapping powers. Note too that α is independent of the trap stiffness in Eq. (26). Finally, we note that while the trapping power dictates the relative strengths of the trap stiffness (conservative) and radiation pressure (nonconservative), it should not modify the ratio of the two competing forces under conditions where the harmonic approximation for the trap stiffness is valid.

The fitting parameters are shown in Table II.

In addition to the characteristic power spectrum described above, another important property observed in this system is its tendency to produce a continuous cycling of the position and orientation under steady state conditions. This cyclic motion was detected using a winding number analysis in which winding events were denoted when the nanowire trajectory moved around the center of the trap in either a clockwise (negative) or anticlockwise (positive) motion. In an unbiased system the rates of cycling in either direction should be

balanced, leading to an average of zero winding. The results presented for different powers in Fig. 6(a) indicate that the nanowires have a tendency to persistently cycle around a central point within the trap in a particular sense; short time-scale fluctuations correspond to Brownian fluctuations in the trend. The winding behavior is persistent over many seconds and is reproducible for each individually trapped wire. The cycling in a particular sense suggests an underlying bias within the trapping geometry, however cycling in the opposite sense is also observed for some trapping events. We find that for different powers the rate of winding increases before plateauing at higher powers; this is clearly observed in a plot of the gradient of the winding number with trapping power, shown in Fig. 6(b). The characteristic frequency of the winding is much less than the frequency of the broad resonance peak and it is not obviously detectable in the power spectra in Fig. 4.

TABLE II. Fitting parameters for power spectrum at different trapping powers.

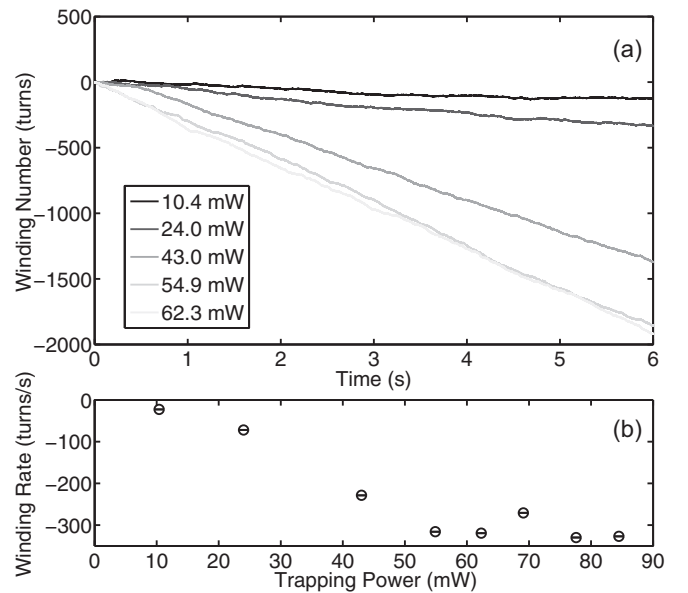| P (mW)	ϵ (Hz^2)	$|\mu|$ (Hz)	β/α	α	σ
10.4	3.819×10^4	213	2.035×10^4	1.379×10^4	0.00016
24.0	3.155×10^5	552	3.000×10^5	1.179×10^4	0.0007
43.0	8.467×10^5	782	5.193×10^5	1.915×10^5	0.009
54.9	1.499×10^6	969	8.977×10^5	4.816×10^5	0.03
62.3	1.871×10^6	1111	1.094×10^6	5.76×10^5	0.03
69.1	2.516×10^6	1375	1.535×10^6	7.798×10^5	0.045
77.6	3.143×10^6	1518	1.877×10^6	5.593×10^5	0.044
84.5	3.935×10^6	1841	2.209×10^6	1.31×10^6	0.096

FIG. 6. (a) A winding number plot of the nanowire motion for different trapping powers. Small time-scale fluctuations in the winding decorate a clear linear increase with time, indicating persistent cycling in one direction. (b) The rate of winding, given by the gradient of the winding plots, is observed to increase approximately trapping power for lower powers and plateau at higher powers.

V. SUMMARY

In this work we have described experimental results and theoretical modeling on the dynamics of high-aspect-ratio nanowires trapped axially in a single gradient force optical tweezers. Experimental measurements of the power spectral density reveal a broad peak of the order of kHz. The position of this peak is blueshifted with increasing input trapping power. A separate analysis of time series data reveals a persistent low frequency cyclical motion, less than one kHz, around the equilibrium trapping position. The frequency of this motion is not readily identifiable in the power spectral density. We introduced a theoretical model for the motion of the nanowire, which incorporates linear restoring optical forces, a nonconservative asymmetric coupling between translational and rotational degrees of freedom, viscous drag, and white noise. This model provides an excellent fit to the experimental power spectral density observations. Our experimental and theoretical results provide clear evidence for either a nonconservative coupling between translational and rotational modes in optical trapped nanowires, or an induced torque arising from low Reynolds viscous drag, or a combination of both. Further experimental and theoretical studies on this model system may be able to elucidate further on these and other complex dynamic behaviours, and this may provide new insights into analogous biophysical systems.

[1] B. M. Mihiretie, P. Snabre, J. C. Loudet, and B. Pouligny, Eur. Phys. J. E **37**, 124 (2014).

[2] G. A. Swartzlander, T. J. Peterson, A. B. Artusio-Glimpse, and A. D. Raisanen, Nat. Photon. **5**, 48 (2011).

[3] S. Sukhov and A. Dogariu, Phys. Rev. Lett. **107**, 203602 (2011).

[4] D. B. Phillips, P. J., S. Hanna, Y. L. D. Ho, D. M. Carberry, M. J. Miles, and S. H. Simpson, Nat. Photon. **8**, 400 (2014).

[5] S. H. Simpson and S. Hanna, Phys. Rev. E **82**, 031141 (2010).

[6] Y. Roichman, B. Sun, A. Stolarski, and D. G. Grier, Phys. Rev. Lett. **101**, 128301 (2008).

[7] I. Saberi and F. Gittes, J. Opt. Soc. Am. B **28**, 2369 (2011).

[8] P. J. Reece, W. J. Toe, F. Wang, S. Paiman, Q. Gao, H. H. Tan, and C. Jagadish, Nano Lett. **11**, 2375 (2011).

[9] F. Wang, W. J. Toe, W. M. Lee, D. McGloin, Q. Gao, H. H. Tan, C. Jagadish, and P. J. Reece, Nano Lett. **13**, 1185 (2013).

[10] S. Simpson, D. Phillips, D. Carberry, and S. Hanna, J. Quant. Spectrosc. Radiat. Transfer **126**, 91 (2013).

[11] A. A. R. Neves, A. Camposeo, S. Pagliara, R. Saija, F. Borghese, P. Denti, M. A. Iatì, R. Cingolani, O. M. Maragò, and D. Pisignano, Opt. Express **18**, 822 (2010).

[12] L. Tong, V. D. Miljković, and M. Käll, Nano Lett. **10**, 268 (2010).

[13] S. Paiman, Q. Gao, H. H. Tan, C. Jagadish, K. Pemasiri, M. Montazeri, H. E. Jackson, L. M. Smith, J. M. Yarrison-Rice, X. Zhang, and J. Zou, Nanotechnology **20**, 225606 (2009).

[14] J. Happel and H. Brenner, *Low Reynolds Number Hydrodynamics* (Noordhoff International Publishing, Leyden, IL, 1973).

[15] C. W. Gardiner, *Handbook of Stochastic Methods for Physics, Chemistry and the Natural Sciences*, 3rd ed., Springer Series in Synergetics Vol. 13 (Springer-Verlag, Berlin, 2004), pp. xviii and 415.

[16] K. Berg-Sorensen and H. Flyvbjerg, Rev. Sci. Instrum. **75**, 594 (2004).

[17] A. Irrera, P. Artoni, R. Saija, P. G. Gucciardi, M. A. Iatì, F. Borghese, P. Denti, F. Iacona, F. Priolo, and O. M. Maragò, Nano Lett. **11**, 4879 (2011).